

Insights into the Incorporation of Signal Information in Binaural Signal Matching with Wearable Microphone Arrays

Ami Berger*, Vladimir Tourbabin[†], Jacob Donley[†], Zamir Ben-Hur[†], Boaz Rafaely*

*School of Electrical and Computer Engineering, Ben-Gurion University of the Negev, Beer-Sheva 84105, Israel

[†]Reality Labs Research @ Meta, Menlo Park, CA 94025, USA

Abstract—The increasing popularity of spatial audio in applications such as teleconferencing, entertainment, and virtual reality has led to the recent developments of binaural reproduction methods. However, only a few of these methods are well-suited for wearable and mobile arrays, which typically consist of a small number of microphones. One such method is binaural signal matching (BSM), which has been shown to produce high-quality binaural signals for wearable arrays. However, BSM may be suboptimal in cases of high direct-to-reverberant ratio (DRR) as it is based on the diffuse sound field assumption. To overcome this limitation, previous studies incorporated sound-field models other than diffuse. However, this approach was not studied comprehensively. This paper extensively investigates two BSM-based methods designed for high DRR scenarios. The methods incorporate a sound field model composed of direct and reverberant components. The methods are investigated both mathematically and using simulations, finally validated by a listening test. The results show that the proposed methods can significantly improve the performance of BSM, in particular in the direction of the source, while presenting only a negligible degradation in other directions. Furthermore, when source direction estimation is inaccurate, performance of these methods degrade to equal that of the BSM, presenting a desired robustness quality.

Index Terms—Binaural Reproduction, Wearable Arrays, Binaural Signal Matching, Directional error, Adaptive Filters.

I. INTRODUCTION

The binaural reproduction of acoustic scenes captured by microphone arrays is gaining popularity in diverse applications, such as teleconferencing and virtual and augmented reality, as evident by recent publications [1]–[3]. A common technique for binaural reproduction involves convolving high-order Ambisonics (HOA) signals with the head-related transfer function (HRTF) [4]. This method is relatively precise, especially for sufficiently high spherical harmonics (SH) orders, and it can provide a realistic immersion experience through the integration of head tracking [2]. However, the primary constraint of this method is the requirement for an extensive number of microphones when the audio signal is captured using a microphone array, as well as the need for a spherical array geometry, which limits the practical application of this method [2].

To address the limitations of binaural signal reproduction with spherical array geometries, the beamforming-based binaural reproduction (BFBR) technique was proposed [5]–[7]. In this method, microphone signals are filtered using

a set of beamformers, followed by filtering with the head-related transfer functions (HRTFs), finally added to produce the binaural signals. A theoretical framework for determining the design parameters of BFBR, such as the number of beams and their look direction for both planar and spherical arrays, was presented in [8]. However, the guidelines for more general array geometries were limited and did not guarantee accurate binaural signal reproduction, leaving a comprehensive design methodology unavailable.

In an effort to overcome the limitations of existing beamforming-based methods and to accurately reproduce binaural signals captured by arrays of arbitrary geometry, a number of techniques have been developed [9]–[12]. The binaural signal-matching (BSM) technique is one such technique [13], [43]. BSM entails estimating the binaural signals directly from the array measurements using least-squares (LS) optimization. To enhance perception, at high frequencies, Magnitude Least-Squares (MagLS) optimization is used instead [26]. A BSM design was recently presented for a semi-circular array with varying numbers of microphones, incorporating head tracking [13]. The study revealed that BSM accuracy heavily depends on microphone positioning, leading to poor performance when a listener’s ear is distant from the recording microphones. In addition, the BSM which is designed under a diffused sound-field assumption may be sub-optimal under high Direct-to-Reverberant Ratio (DRR) conditions, for example [29].

Parametric spatial audio was also investigated as an alternative for binaural reproduction. In these approaches, the sound field is decomposed into direct and reverberant components, each estimated and reproduced independently [21]–[25]. While this approach has shown promising results, its accuracy depends on the estimation of signal-dependent model parameters, such as the direction-of-arrival (DOA) of sound sources, and the direct-to-reverberant ratio (DRR) of the sound field. This drawback of the parametric approach, and the limitations of the beamforming approach detailed above, define the current gaps in binaural reproduction using arrays of arbitrary configurations, highlighting the need for improved solutions.

This paper aims to address the shortcomings of current methods by exploring the incorporation of signal information into BSM. The potential benefit would be high stability and fidelity due to the nature of the BSM linear filtering, with

improvement in performance at high frequency and due to head rotation delivered by modeling sound sources. Two relevant approaches have been recently proposed. The first is to incorporate signal information in the correlation matrix employed in the BSM design [29], and the second is based on parametric spatial coding, e.g. COMPASS [25], where the residual sound field complementing individual source modeling is reproduced using a BSM like approach. While both approaches showed promising potential, it is unclear from current literature which is preferred, or in general, what is the best way to incorporate signal information into BSM.

This paper presents a comprehensive theoretical formulation and experimental investigation to cover this gap. The work is a significant extension of a conference paper by the same authors that investigated the feasibility of incorporating signal information into BSM [44]. The work shows both methods exhibit commendable performance when the array microphones are in close proximity to the ears of a listener virtually positioned in the sound scene. However, the performance degrades as the microphones move further from the listener ears. Furthermore, a novel performance metric is employed to analyze the expected relative errors associated with each approach across different directions. The main contributions of this paper are:

- 1) A new performance metric of BSM is proposed. This metric quantifies the expected relative error as a function of sound source direction. The metric is referred to as the “directional error”. Utilizing this metric, it becomes evident that the BSM exhibits distinct errors that are dependent on the DOA of the sound sources, highly related to HRTF magnitude. This behavior is further validated using interaural time difference (ITD) and interaural level difference (ILD) analysis.
- 2) The presentation, analysis, and comparison of two distinct approaches that incorporate signal information into the BSM method, in particular information on source DOA. These methods are shown to overcome the limitations imposed by the directional behavior of the BSM, performing well for all source directions. This behavior is also validated through ITD and ILD analysis.
- 3) Furthermore, performance analysis of the methods reveals a discernible trade-off, wherein the enhancement of BSM performance in the DOA of a sound source is counterbalanced by only a marginal decrement in performance across most other directions. In particular, one method performs better in directions away from the source. This method was also found to be more robust to errors in the estimation of the source DOA.
- 4) Finally, a comprehensive simulation study and a listening experiment are performed that substantiate the accuracy and quality of the different methods with a wearable microphone array, validating the methods behavior and limitations.

II. MATHEMATICAL BACKGROUND

A. Signal Model

This subsection provides the mathematical model of the signal as used in this paper. Throughout the paper, the standard spherical coordinate system is used, denoted by (r, θ, ϕ) , where r is the distance to the origin, θ is the elevation angle measured from the Cartesian z axis downwards to the Cartesian xy plane, and ϕ is the azimuth angle measured from the positive x axis towards the positive y axis. We denote $k = \frac{2\pi}{\lambda}$ as the wave-number, where λ is the wave-length, f is the frequency and $\Omega = (\theta, \phi)$ represents the arrival direction of a plane wave in the sound field. Further, assume that the sound-field is composed of L far-field sound sources generating plane waves with arrival directions $\Omega_l, l = 1, \dots, L$, and source signals $s_l(f), l = 1, \dots, L$ [14]. The sound-field is captured by an array of M microphones, which are located at $(r_m, \Omega_m), m = 1, \dots, M$, centered at the origin. The noisy array measurements can therefore be described by the following narrow-band model [14]:

$$\mathbf{x}(f) = \mathbf{V}(f)\mathbf{s}(f) + \mathbf{n}(f) \quad (1)$$

where $\mathbf{x}(f) = [x_1(f), x_2(f), \dots, x_M(f)]^T$ is the microphone-signal vector (measurements), $\mathbf{V}(f) = [\mathbf{v}(k, \Omega_1), \mathbf{v}(k, \Omega_2), \dots, \mathbf{v}(k, \Omega_L)]$ is an $M \times L$ complex matrix with columns $\mathbf{v}(k, \Omega_l)$ representing the array steering vector from the l -th source to the microphone positions for all $l = 1, \dots, L$ sources, $\mathbf{s}(f) = [s_1(f), s_2(f), \dots, s_L(f)]^T$ is the source-signal vector, and $\mathbf{n}(f)$ is an additive-noise vector.

In the BSM model we further assume that a listener is virtually positioned with the center of the head coinciding with the origin, where $h^{l,r}(k, \Omega)$ denotes the HRTF of the left and right ears of the listener using the superscripts $(\cdot)^l$ for the left ear and $(\cdot)^r$ for the right ear. The signal at the left and right ears can now be written as [37]:

$$p^{l,r}(f) = [\mathbf{h}^{l,r}(f)]^T \mathbf{s}(f) \quad (2)$$

where $\mathbf{h}^{l,r} = [h^{l,r}(\Omega_1), h^{l,r}(\Omega_2), \dots, h^{l,r}(\Omega_L)]^T$ contains the HRTFs corresponding to the directions of the sources.

B. Binaural Signal Matching

This subsection provides the mathematical model of BSM. First, assume that the configuration of the microphone array is known, such that the steering matrix $\mathbf{V}(f)$ can be generated by simulation or measurement. In the first step, the array measurements are filtered and combined, in a similar manner to beamforming:

$$\hat{p}^{l,r}(f) = [\mathbf{c}^{l,r}(f)]^H \mathbf{x}(f) \quad (3)$$

where \mathbf{c} is an $M \times 1$ complex vector holding the filter coefficients. Next, \mathbf{c} is chosen to minimize the following mean-squared error between $\hat{p}^{l,r}(f)$ and $p^{l,r}(f)$, the binaural signals in (2), for each ear separately:

$$err_{bin}^{l,r}(f) = \mathbb{E}[|p^{l,r}(f) - \hat{p}^{l,r}(f)|^2] \quad (4)$$

where $\mathbb{E}[\cdot]$ is the expectation operator. Next, assume that the noise is uncorrelated to the sources. This leads to the following error formulation [13]:

$$\begin{aligned} err_{bin}^{l,r}(f) = & \mathbb{E}[\|[\mathbf{s}(f)]^H([\mathbf{V}(f)]^H \mathbf{c}^{l,r}(f) - [\mathbf{h}^{l,r}(f)]^*)\|^2 \\ & + \|[\mathbf{n}(f)]^H \mathbf{c}^{l,r}(f)\|^2] \end{aligned} \quad (5)$$

Eq. (5) can also be written in a matrix form, omitting the explicit dependence on frequency, as:

$$\begin{aligned} err^{l,r} = & ((\mathbf{c}^{l,r})^H \mathbf{V} - [\mathbf{h}^{l,r}]^T) \mathbf{R}_s (\mathbf{V}^H \mathbf{c}^{l,r} - [\mathbf{h}^{l,r}]^*) \\ & + (\mathbf{c}^{l,r})^H \mathbf{R}_n \mathbf{c}^{l,r} \end{aligned} \quad (6)$$

Minimizing the error in Eq. (6) leads to the following solution:

$$\mathbf{c}_{opt}^{l,r}(f) = (\mathbf{V} \mathbf{R}_s \mathbf{V}^H + \mathbf{R}_n)^{-1} \mathbf{V} \mathbf{R}_s [\mathbf{h}^{l,r}]^* \quad (7)$$

where $\mathbf{R}_s = E[\mathbf{s}\mathbf{s}^H]$, $\mathbf{R}_n = E[\mathbf{n}\mathbf{n}^H]$. Next, if \mathbf{R}_s is unknown, one can assume that the sound field is diffuse as in [20], leading to $\mathbf{R}_s = \sigma_s^2 \mathbf{I}_L$ and with sources DOA uniformly spread around the sphere. Additionally, it is assumed that the noise is uncorrelated across microphones and identically distributed, such that $\mathbf{R}_n = \sigma_n^2 \mathbf{I}_M$, where σ_n^2 is the noise variance, σ_s^2 is the source variance and $\mathbf{I}_M, \mathbf{I}_L$ are the $M \times M$ and $L \times L$ identity matrices, respectively. These assumptions lead to the following simplification of Eq. (7) [13]:

$$\mathbf{c}_{BSM}^{l,r}(f) = (\mathbf{V} \mathbf{V}^H + \frac{1}{SNR} \mathbf{I}_M)^{-1} \mathbf{V} [\mathbf{h}^{l,r}]^* \quad (8)$$

where $SNR = \frac{\sigma_s^2}{\sigma_n^2}$.

To reduce the negative impact of spatial cues at high frequencies becoming less accurate because of the loss of precision in BSM and increase in binaural error, it was suggested in [20] to modify BSM at high frequencies by minimizing the magnitudes in Eq. (5) using MagLS [26]. It was based on the idea that ILD is more noticeable than ITD for spatial perception at high frequencies [30]- [31]. In [20] it was shown that even with the use of MagLS the BSM still has a high error for high frequencies and that the performance rapidly degrades the further the microphones are from the ears of a virtual listener. In addition, in cases where the sound-field is directional, such as a speaker in a room, the diffuse sound-field assumption made in the development of the BSM fails which may lead to even higher errors. In this paper, methods that aim to improve the BSM method, especially in cases of directional sound-fields will be presented and analysed.

III. BSM APPROACHES THAT INCORPORATE SIGNAL INFORMATION

This section introduces two distinct BSM-based binaural reproduction approaches. These approaches incorporate signal information, specifically modeling dominant sound sources, extending beyond the solution provided in Eq. (8), which assumes a diffuse field. Throughout this section it is assumed that the sound-field, described in Eq. (1), is composed of direct and reverberant components. The direct component is composed of the direct sound from D far-field sources corresponding to a DOA of $\boldsymbol{\Omega}_d = [\Omega_1, \dots, \Omega_D]^T$. The reverberant

component is approximated to be composed of L far-field sources whose DOA's are uniformly spread on a sphere as in the model presented in Section II-B. This leads to the following formulation of the signal model:

$$\mathbf{x}(f) = \mathbf{V}_d \mathbf{s}_d + \mathbf{V}_r \mathbf{s}_r + \mathbf{n} \quad (9)$$

where \mathbf{V}_d is the $M \times D$ steering matrix of the direct component, \mathbf{V}_r is the $M \times L$ assumed steering matrix for the reverberant component, and \mathbf{s}_d and \mathbf{s}_r are the source signal vectors for the direct and reverberant components, respectively. It is further assumed that the measurement noise \mathbf{n} is white, uncorrelated to the source signals and that $\mathbb{E}[\mathbf{n}\mathbf{n}^H] = \sigma_n^2 \mathbf{I}_M$. Throughout this section, the following parameters are assumed to be separately estimated:

- The DOA of the D direct sources, $\boldsymbol{\Omega}_d$. Throughout this section, the dependency on $\boldsymbol{\Omega}_d$ for the direct component is omitted for simplicity.
- The measurements correlation matrix $\mathbf{R}_x = \mathbb{E}[\mathbf{x}\mathbf{x}^H]$.

It is also assumed that the source signals of the direct component are estimated by applying a linearly-constrained minimum-variance (LCMV) beamformer [32]:

$$\hat{\mathbf{s}}_d = \mathbf{W}_d \mathbf{x} \quad (10)$$

where \mathbf{W}_d is the weights matrix calculated using the constraint $\mathbf{W}_d \mathbf{V}_d = \mathbf{I}_D$ where \mathbf{I}_D is a $D \times D$ identity matrix, as shown in [32] which leads to:

$$\mathbf{W}_d = (\mathbf{V}_d^H (\mathbf{R}_x)^{-1} \mathbf{V}_d)^{-1} \mathbf{V}_d^H (\mathbf{R}_x)^{-1} \quad (11)$$

Note that because the LCMV is computed with correlation matrix \mathbf{R}_x , it is assumed that \mathbf{s}_d is uncorrelated to \mathbf{s}_r which is required to avoid signal cancellation [38].

A. BSM Incorporated with Parametric Spatial Coding

This subsection outlines a mathematical model that integrates a parametric spatial coding method with the BSM technique for an arbitrary array. This approach will be referred to as COMPASS-BSM (COM) [45], [46]. In this approach it is assumed that the measured signal can be described by Eq. (9). Using the estimated $\hat{\mathbf{s}}_d$, the binaural signal for the direct component can be calculated as follows Eq. (2):

$$\hat{p}_d^{l,r} = [\mathbf{h}_d^{l,r}]^T \hat{\mathbf{s}}_d \quad (12)$$

where $\hat{p}_d^{l,r}$ represents the binaural signal for the direct component at the ears and $\mathbf{h}_d^{l,r}$ denote the HRTF vectors associated with the direct component.

With the estimated $\hat{\mathbf{s}}_d$, the reverberant plus noise component of the measurement can be estimated by substituting Eq. (10) into Eq. (9), as:

$$\hat{\mathbf{x}}_r = (\mathbf{I}_M - \mathbf{V}_d \mathbf{W}_d) \mathbf{x} \quad (13)$$

Next, using $\hat{\mathbf{x}}_r$, the reverberant component of the binaural signal, $\hat{p}_r^{l,r}$, can be estimated using the BSM method as in Eq. (3):

$$\hat{p}_r^{l,r} = (\mathbf{c}_{BSM}^{l,r})^H \hat{\mathbf{x}}_r \quad (14)$$

where $\mathbf{c}_{BSM}^{l,r}$ are the standard BSM weights which are calculated as shown in Section II-B.

Finally, the binaural signal for the entire sound field is calculated as the sum of the binaural signals for the direct and reverberant components:

$$\hat{p}^{l,r} = \hat{p}_d^{l,r} + \hat{p}_r^{l,r} \quad (15)$$

where the resulting filter weights can be written by substituting Eqs. (12) and (14) into (15), as:

$$\mathbf{c}_{COM}^{l,r}(\boldsymbol{\Omega}_d, f) = (\mathbf{I}_M - \mathbf{V}_d \mathbf{W}_d)^H \mathbf{c}_{BSM}^{l,r} + \mathbf{W}_d^H [\mathbf{h}_d^{l,r}]^* \quad (16)$$

where $\mathbf{c}_{BSM}^{l,r}$ are defined in Eq. (14), such that:

$$\hat{p}^{l,r} = (\mathbf{c}_{COM}^{l,r})^H \mathbf{x} \quad (17)$$

B. BSM with Informed Correlation Matrix

In this subsection, a BSM-based binaural reproduction approach that incorporates the direct component information into the source correlation matrix is introduced with the goal of better estimating the optimal filter described in Eq. (7). This approach will be referred to as Directional BSM (d-BSM). In this approach it is assumed that the measured signal can be described by Eq. (9); that \mathbf{s}_d and \mathbf{s}_r are uncorrelated; and that $\mathbb{E}[\mathbf{s}_r \mathbf{s}_r^H] = \sigma_r^2 \mathbf{I}_L$, where \mathbf{I}_L is the $L \times L$ identity matrix and σ_r^2 is the assumed variance of the sources belonging to the reverberant component. Note that the latter assumption holds when the reverberant component is diffuse. Using $\hat{\mathbf{s}}_d$ as in Eq. (10) the covariance matrix of the sources belonging to the direct component can be estimated as:

$$\hat{\mathbf{R}}_{\mathbf{s}_d} = \mathbb{E}[\hat{\mathbf{s}}_d \hat{\mathbf{s}}_d^H] \quad (18)$$

Using $\hat{\mathbf{x}}_r$ as in Eq. (13), the equivalent variance of the sources belonging to the reverberant component can be estimated as:

$$\hat{\sigma}_r^2 = \frac{1}{L} \|\hat{\mathbf{x}}_r\|_2^2 \quad (19)$$

Next, the sources covariance matrix, \mathbf{R}_s can be estimated from Eqs. (18) and (19) as:

$$\hat{\mathbf{R}}_s = \begin{bmatrix} \hat{\mathbf{R}}_{\mathbf{s}_d} & \mathbf{0} \\ \mathbf{0} & \hat{\sigma}_r^2 \mathbf{I}_L \end{bmatrix} \quad (20)$$

Now, by substituting $\hat{\mathbf{R}}_s$ in Eq. (7), the optimal filter can be computed as:

$$\mathbf{c}_{d-BSM}^{l,r}(\boldsymbol{\Omega}_d, f) = \mathbf{B}^{-1} (\mathbf{V}_d \hat{\mathbf{R}}_{\mathbf{s}_d} [\mathbf{h}_d^{l,r}]^* + \hat{\sigma}_r^2 \mathbf{V}_r [\mathbf{h}_r^{l,r}]^*) \quad (21)$$

where $\mathbf{h}_r^{l,r}, \mathbf{h}_d^{l,r}$ denote the HRTF vectors associated with the reverberant and direct components, respectively, $\mathbf{c}_{d-BSM}^{l,r}(\boldsymbol{\Omega}_d)$ is the filter weight vector and \mathbf{B} is calculated as:

$$\mathbf{B} = \hat{\sigma}_r^2 \mathbf{V}_r \mathbf{V}_r^H + \mathbf{V}_d \hat{\mathbf{R}}_{\mathbf{s}_d} \mathbf{V}_d^H + \sigma_n^2 \mathbf{I}_M \quad (22)$$

As in the standard BSM, at high frequencies, MagLS [26] can be used to minimise Eq. (5). Observing Eq. (5) it can be noted that it can equivalently be written as:

$$\begin{aligned} err_{bin}^{l,r}(\boldsymbol{\Omega}_d, f) &= \|\mathbf{R}_s^{0.5}([\mathbf{V}]^H \mathbf{c}^{l,r} - [\mathbf{h}^{l,r}]^*)\|_2^2 \\ &+ \|\mathbf{R}_n^{0.5} \mathbf{c}^{l,r}\|_2^2 \end{aligned} \quad (23)$$

Where $\mathbf{V} = [\mathbf{V}_d, \mathbf{V}_r]$ and $\mathbf{h}^{l,r} = [\mathbf{h}_d^{l,r}; \mathbf{h}_r^{l,r}]$. By substituting Eq. (18) into Eq. (23) the MagLS formulation can be written as:

$$\begin{aligned} \mathbf{c}_{d-BSM}^{l,r}(\boldsymbol{\Omega}_d, f) &= \arg \min_{\mathbf{c}} \left\| |\hat{\mathbf{R}}_s^{0.5} \mathbf{V}^H \mathbf{c}^{l,r}| - |\hat{\mathbf{R}}_s^{0.5} [\mathbf{h}^{l,r}]^*| \right\|_2^2 \\ &+ \sigma_n^2 \|\mathbf{c}^{l,r}\|_2^2 \end{aligned} \quad (24)$$

C. Distinction between the two approaches

This subsection aims to provide some insight into the differences between the two approaches. The first method separates direct and reverberant components to provide a better model for the reverberant component but may be sensitive to estimation errors. Conversely, the second method estimates only the variance of the reverberant component without needing to estimate this component's signal. It is therefore expected to be more robust against estimation errors. Essentially, the trade-off between the two methods lies in the detail of modeling and robustness to estimation error.

IV. ERROR MEASURES

This section introduces the main error measures that are used throughout this paper to evaluate and compare the different binaural reproduction methods.

A. Normalised Mean-Square Error

The normalized mean-squared error (NMSE) of the binaural signals is calculated as:

$$NMSE^{l,r}(f) = \begin{cases} \frac{|\hat{p}^{l,r}(f) - p_{ref}^{l,r}(f)|^2}{|p_{ref}^{l,r}(f)|^2}, & \text{for } f < 1.5\text{kHz} \\ \frac{||\hat{p}^{l,r}(f)| - |p_{ref}^{l,r}(f)||^2}{|p_{ref}^{l,r}(f)|^2}, & \text{for } f \geq 1.5\text{kHz} \end{cases} \quad (25)$$

where $p_{ref}^{l,r}(f)$ is the reference binaural signal of a certain frequency, and $\hat{p}^{l,r}(f)$ is the reproduced binaural signal of the same frequency. For frequencies above 1.5 kHz the NMSE of the absolute value was calculated based on magnitude only, aligning with sound perception, as shown in [20].

B. Directional Error

This subsection introduces a novel measure to analyze the BSM method, referred to as the directional error. Additionally, a methodology for computing this error is provided. For simplicity, throughout this section the dependency on the frequency is omitted. Assume the BSM filter \mathbf{c} is computed as outlined in Section II-B, and that the sound-field described in Section II-A consists solely of a single source, having a DOA denoted as Ω . Additionally, assume that the source signal s is wide sense stationary. Next, the directional error at frequencies below 1.5 kHz is defined as the normalized mean square error, as a function of the source signal DOA. This error can be calculated under these assumptions using Eq. (4),

further assuming no noise and finally applying normalization, as follows:

$$err_{dir}^{l,r}(\Omega) = \begin{cases} \frac{\|\mathbf{v}(\Omega)^H \mathbf{c}^{l,r} - [h^{l,r}(\Omega)]^*\|_2}{|h^{l,r}(\Omega)|}, & \text{for } f < 1.5\text{kHz} \\ \frac{\|[\mathbf{v}(\Omega)]^H \mathbf{c}^{l,r} - |h^{l,r}(\Omega)|\|_2^2}{|h^{l,r}(\Omega)|^2}, & \text{for } f \geq 1.5\text{kHz} \end{cases} \quad (26)$$

where $err_{dir}^{l,r}(\Omega)$ refers to the directional error for the left and right channels, $\mathbf{c}^{l,r}$ is the BSM filter, $h^{l,r}(\Omega)$ refers to the HRTF with direction Ω , and $\mathbf{v}(\Omega)$ is a $M \times 1$ complex array steering vector corresponding to a given DOA. For high-frequency signals, due to consideration of sound perception [39], the directional error is based on signal magnitude.

C. ITD and ILD

In this subsection, performance measures based on ITD and ILD are outlined. Throughout this section, it is assumed that the sound-field, as described in Section II-A, comprises solely of a single source, having a DOA denoted as Ω , with a unit variance. Using Eq. (3), both $p^l(t)$ and $p^r(t)$, representing the left and right time-domain binaural signals, were computed for a chosen BSM filter. The reference binaural signals were derived by substituting the source signal in Eq. (2).

The ITD computation employed a well-accepted perceptual measure [33], utilizing a cross-correlation based method. Initially, the binaural signals were low-pass filtered at a cutoff frequency of 1.5 kHz, followed by the ITD calculation depicted as:

$$ITD(\Omega) = \arg \max_{\tau} \left| \sum_{t=0}^{T-\tau-1} p^r(t)p^l(t+\tau) \right| \quad (27)$$

where T represents the total number of time samples. The chosen cutoff frequency of 1.5 kHz aligns with the frequency range crucial for spatial perception through phase or binaural time differences.

After computing ITD for both the BSM filter and the reference signal, the ITD error measure was computed as:

$$\epsilon_{ITD}(\Omega) = |ITD(\Omega) - ITD_{ref}(\Omega)| \quad (28)$$

For the ILD estimation, the binaural signals was processed using ERB filter bands, as outlined in [34]:

$$ILD_f(f_c, \Omega) = 10 \log_{10} \frac{\sum_{f=0}^{f_c^{max}} |G(f, f_c)p^l(f)|^2}{\sum_{f=0}^{f_c^{max}} |G(f, f_c)p^r(f)|^2} \quad (29)$$

where $G(f, f_c)$ represents the ERB filter with central frequency f_c at frequency f , and f_c^{max} denotes the maximum frequency of this ERB filter. An average of 22 filter bands in the [1.5, 20] kHz range, generated using the Auditory Toolbox [35], was used to compute ILD as:

$$ILD(\Omega) = \frac{1}{22} \sum_{f_c} ILD_f(f_c, \Omega) \quad (30)$$

Subsequently, the ILD error measure was computed as:

$$\epsilon_{ILD}(\Omega) = \frac{1}{22} \sum_{f_c} |ILD_f(f_c, \Omega) - ILD_{ref}(f_c, \Omega)| \quad (31)$$

V. SIMULATION STUDY

In this section, a comparison between the two approaches, presented in Section III, and the standard BSM, presented in Section II-B, is provided. Broadly, this section aims to study the benefits and to gain insights into signal-dependent BSM approaches, in particular studying direction-dependent performance highlighting the points made in Section III-C regarding the methods modeling detail and robustness to error.

A. Simulation Set-Up

In this section, a semi-circular microphone array, mounted on a rigid sphere, comprising $M = 6$ omnidirectional microphones arranged on the horizontal plane was simulated. The semi-circular array was chosen since it is a simplified representation of a head-worn array, such as augmented reality glasses. The microphone positions were denoted using spherical coordinates $(r, \frac{\pi}{2}, \phi_m)$ for $m = 1, \dots, M$ relative to the array center, where $r = 10$ cm and $\phi_m = \frac{\pi}{2} - \frac{\pi(m-1)}{M-1}$ rad. The steering vectors of this array were computed analytically in the SH domain following section 4.2 in [16] using the array geometry and the DOAs of the far-field sources modeled as plane waves. The HRTF in the simulation was obtained from the Cologne database measurements of the Neumann KU100 manikin [17]. The HRTFs for the DOAs of the assumed sources were interpolated in the SH domain using a SH order of 30. The assumed listener head was aligned with the positive x axis. An illustration of the array position relative to the head position and alignment is presented in Figure 1. An orientation of 90° as shown in Figure 1(c) of the array relative to the head was found to be the most challenging for the BSM algorithm [20] since the right ear is relatively far from any of the arrays microphones compared to the standard case of no head rotation as shown in 1(a).

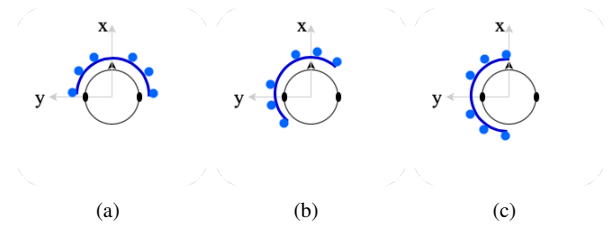


Fig. 1. An illustration of a virtual listener head and the semi-circular array assuming a: 1(a) 0° array rotation. 1(b) 50° array rotation. 1(c) 90° array rotation. The blue dots represent the array microphones, and the x and y grey arrows represent the positive x and y axes, respectively.

Next, three different scenarios were simulated. In all three scenarios a point source was simulated inside a room using the image method [18]. The semi-circular microphone array was centered at a position inside the room facing the x axis as in Figure 1(a). The remaining details of the three simulated scenarios are presented In Table I.

Scenario's 1 and 2 source signals were taken from the TIMIT database [19], and all signals were sampled at 48 kHz.

	Scenario 1	Scenario 2	Scenario 3
Source Signal	Female Speech	Male Speech	Castanets
Duration (s)	5	10	7.5
Array Position (m)	(4, 3, 1.7)	(1.5, 2, 1.7)	(4, 3, 1.7)
Source Distance from Array (m)	0.6	0.9	0.8
Room Dimensions (m)	6 × 4 × 3	7 × 5 × 3	8 × 6 × 4
T_{60} (s)	0.69	0.65	0.64

TABLE I
SIMULATION PARAMETERS

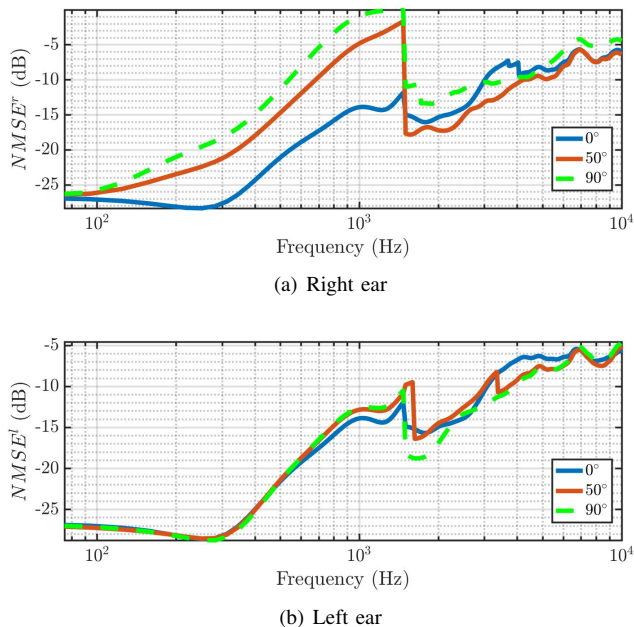


Fig. 2. The NMSE of the BSM method is presented in the top and bottom figures for the right and left ears, respectively. The NMSE values are computed as defined in Section IV-A, with reference to a diffuse sound field as detailed in [20]. The evaluations consider an SNR of 20 dB and three head-rotation of 90°, 50° and no head rotation.

B. Methodology

In this study, $\mathbf{c}_{BSM}^{l,r}$ was computed following Eq.(8) as detailed in Section II-B, and MagLS [26] was employed for frequencies within the range of [1.5, 24] kHz. The steering matrix was computed assuming $L = 400$ sources nearly-uniformly distributed on a sphere according to [15], as elaborated in Section II-B. The MagLS solution was obtained using the variable exchange method [36] with an initial phase of 90°, a tolerance of 10^{-20} , and a maximum of 10^5 iterations. The steering vector of the direct component with a DOA of Ω_d was computed from the source and array positions (see Table I). Subsequently, after generating microphone signals, $\mathbf{x}(t)$, as described in section V-A, $\mathbf{x}[t, f]$ was computed using Short-Time Fourier Transform (STFT) with a Bartlett window of duration 0.032 s and a hop size of 0.008 s. Following this, the measurements' correlation matrix \mathbf{R}_x was computed by averaging across both time and frequency domains according to:

$$\hat{\mathbf{R}}_x[f] = \frac{1}{T} \sum_{t=1}^T \sum_{j=-J}^J \mathbf{x}[t, f + j \cdot \Delta f] \mathbf{x}^H[t, f + j \cdot \Delta f] \quad (32)$$

where T denotes the total length in seconds of the recording, Δf is the frequency resolution and J controls the bandwidth of the frequency smoothing. Subsequently, the LCMV beamformer was computed following Eq. (11), leading to the determination of $\mathbf{c}_{COM}^{l,r}(\Omega_d, f)$ using $\mathbf{c}_{BSM}^{l,r}$, as per Eq. (16) in Section III-A. Further, $\mathbf{c}_{d-BSM}^{l,r}(\Omega_d, f)$ was calculated following the equations outlined in Section III-B, employing the BSM steering matrix as the reverberant component's steering matrix and utilizing MagLS [26] for frequencies within the range of [1.5, 24], kHz.

Following the computation of the three filters, the binaural signals for all filters were computed using Eq. (3) by replacing the appropriate filter $\mathbf{c}^{l,r}$. The reference binaural signals, were calculated by convolving the HRTFs of the left and right ears with the HOA signals of order 14 that were calculated using the image method as described in section V-A. Finally, the errors measures as presented in Section IV were computed using the binaural signals for the three methods, and the reference binaural signals.

C. BSM Directional-Error

This section presents the NMSE of the standard BSM method, as defined in Section IV-A, assuming a diffuse sound field as detailed in [20]. Figure 2 presents this NMSE as a function of frequency for three different head rotations as described in Section V-B.

As can be observed in Figure 2, the error is characterised by a lower errors in low frequencies compared to high frequencies and by a higher error for that ear that is further from the array, i.e. the right ear. This error presents the overall error due to a diffuse sound field and does not provide information on the directional characteristics of the BSM method.

In order to better understand the directional behavior of the BSM method, the directional error, as defined in Section IV-B, is presented in this section. Figures 3 presents the directional error on the horizontal plane assuming an elevation of 90° as a function of frequency for the BSM method assuming no head rotation as described in Section V-B. An abrupt change in the frequency of 1.5 KHz can be observed as this is the MagLS cutoff frequency described in Section V-B. It can also be observed that the error changes quite significantly as a function of direction and frequency. While the error is consistently low below about 1kHz, it changes significantly with azimuth direction at higher frequencies. Figure 4 presents the HRTF magnitude as a function of direction and frequency using a flipped color map compared to Figures 3. It can be observed that the error in Figures 3 resembles the HRTF magnitude in Figure 4 when using this flipped color-map. This means that the error is high at directions where the HRTF magnitude is small. This behavior may become a limitation suggesting higher error at the far ear due to the head shadowing effect.

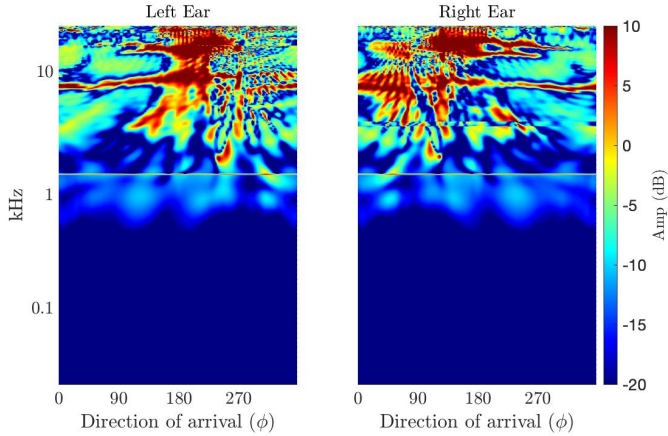


Fig. 3. Surface plots illustrating the directional error of the BSM method, with the left ear presented on the left and the right ear on the right. The directional error is computed in accordance with Section IV-B, considering a consistent elevation of 90° . The frequency is represented on the y-axis, while the azimuth angle ϕ in degrees is depicted on the x-axis, assuming no head rotation.

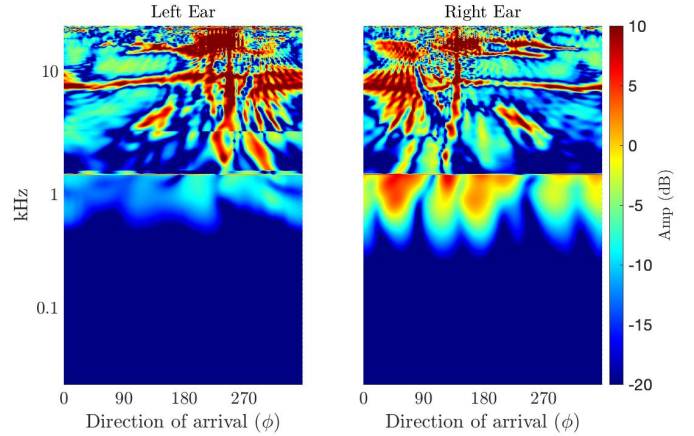


Fig. 5. Surface plots illustrating the directional error of the BSM method, with the left ear presented on the left and the right ear on the right. The directional error is computed in accordance with Section IV-B, considering a consistent elevation of 90° . The frequency is represented on the y-axis, while the azimuth angle ϕ in degrees is depicted on the x-axis, assuming a 50° head rotation.

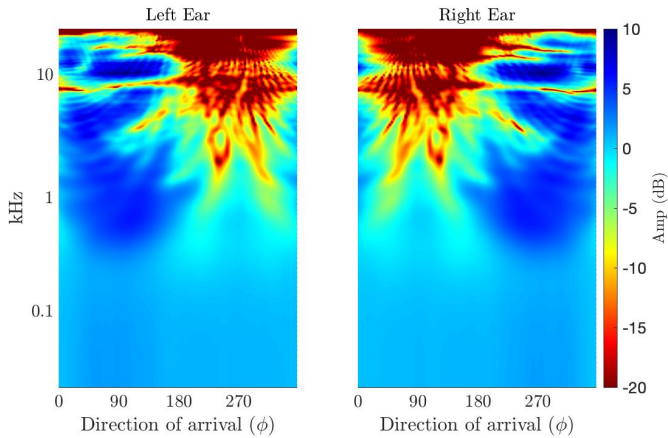


Fig. 4. Surface plots of the magnitude of the HRTF using a flipped color-map, assuming a constant elevation of 90° , where the y axis is the frequency and the x axis is the azimuth angle ϕ in degrees. The HRTF in the simulation was obtained from the Cologne database [17] measurements of the Neumann KU100 manikin. The HRTFs for the DOAs of the assumed sources were interpolated in the SH domain using a SH order of 30.

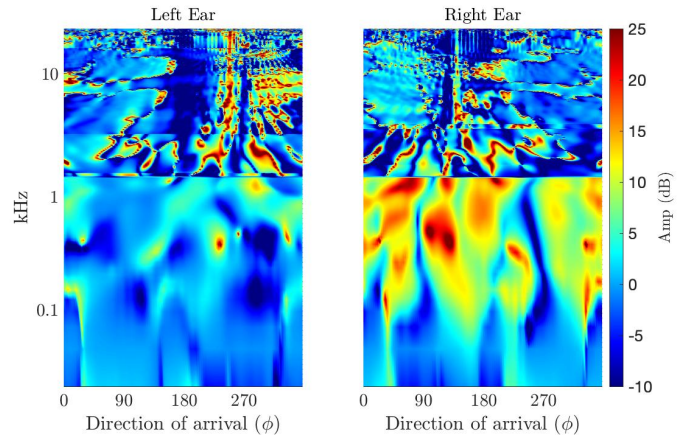


Fig. 6. Surface plots illustrating the increase in error per direction of the BSM method with a 50° head rotation compared to no rotation, i.e. the difference between Figure 5 and Figure 3. The left ear is presented on the left, and the right ear on the right, both maintaining a consistent elevation of 90° . The y-axis corresponds to frequency, while the x-axis represents the azimuth angle ϕ in degrees.

Figure 5 presents the directional error on the horizontal plane assuming an elevation of 90° for various frequencies for the BSM method assuming a 50° head rotation. In the case of 50° head rotation the right ear moves away from the array while the left ear remains relatively close to the array as illustrated in Figure 1. The directional error of the left ear does not change by much compared to Figures 3, while a clear increase in the directional error can be observed for the right ear, as further illustrated next.

Figure 6 presents the difference between Figures 5 and 3.

Upon examination of Figure 6, it becomes evident that the increase in NMSE error associated with the head rotation of 50° , as illustrated in Figure 2, exhibits a directional pattern. Additionally, a closer look at Figure 4 and 6 reveals that the predominant portion of the NMSE error stemming from head rotation, can be linked to directions characterized by small HRTF magnitudes.

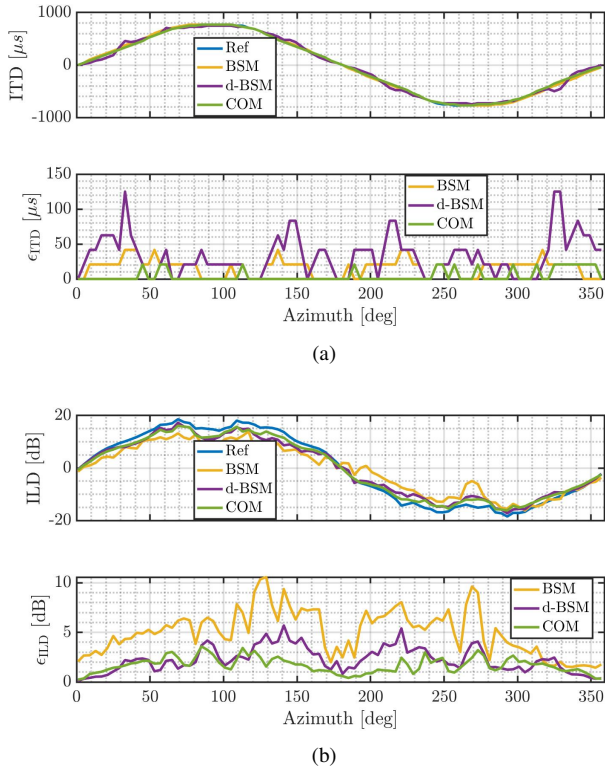


Fig. 7. The ITD (a) and ILD (b) evaluated using the direct sound component of scenario 1 in Table I. The orange line represents the BSM method, the purple line corresponds to the d-BSM approach, and the green line depicts the COM approach. ITD and ILD errors are also presented, as defined in Section IV-C. No head rotation was employed.

D. Analysis of ITD and ILD

Performance metrics studied thus far are rooted in the Mean Squared Error (MSE). However, this might not fully capture human perception. Therefore, a study employing perceptually driven measures, ITD and ILD, is introduced. The ILD and ITD, as outlined in Section IV-C, are presented in this section, for scenarios detailed in Table I comparing the different methods.

The calculation of the ILD and ITD can be divided into two parts. First, a source in a room was simulated generating a scenario in Table I. The recorded signals at the array were then used to compute filters for the methods as described in Section V-B. Now, using the same filters, binaural signals were computed but this time for a sound field composed of a single source in free-field, with the same direction of the source in the room in Table I, and ILD and ITD were calculated as defined in Section IV-C, for this specific source direction. Finally, this same process of computing filters and then ILD and ITD, was repeated for a range of source directions to complete the ILD and ITD analysis. This somewhat non-standard analysis was employed so that the filters could be computed using realistic signals, but then evaluated in terms ILD and ITD in the direction of the source only, as the direct sound is known to dominate sound localization.

Figure 7 illustrates the performance of ILD and ITD as

detailed above for the three distinct methods in scenario 1, as outlined in Table I. The source direction was set on the horizontal plane with an elevation of 90° , and no rotation of the head was considered. The figure shows that all three methods perform reasonably well in terms of ITD, and for most directions remain below the just notable difference (JND) of $100\mu s$ [40]. Furthermore, both novel approaches outperformed the BSM method in terms of ILD with the COM method performing the best. However, for all methods error is mostly above the JND of 1dB [40].

Figure 8(a) illustrates the performance of ILD and ITD under the same conditions of Figure 7, but with 50° head rotation. The figure shows that ILD and ITD error increased significantly for the BSM method and insignificantly for the other two methods. Furthermore, it is noticeable that the error did not uniformly increase across all directions, demonstrating the directional NMSE performance elucidated in Section V-C. This shows the superior performance of the d-BSM and COM methods in terms of ITD and ILD when considering head rotation. This can be explained by the explicit information of the source direction embedded in these two methods.

Figures 8 illustrates the performance of ILD and ITD under the same conditions of Figure 8(a), but for the different scenarios outlined in Table I. As shown in Figures 8, the performance of the different approaches remains consistent across the various scenarios. This result helps to generalize the results of the adaptive filters shown in this section.

E. Robustness to DOA Estimation Errors

In this subsection the ITD and ILD performance will be evaluated assuming an error in the estimation of source direction. Maintaining performance under such conditions is important as some estimation error is expected in practice. Assuming Ω_d is the true DOA of the source, the methods under study will be employed assuming the source has a DOA of $\Omega_d + \Omega_{err}$ where Ω_{err} is the assumed error in the DOA estimation.

Figures 9 presents the ILD and ITD for the methods under study, assuming an elevation of 90° with 50° head rotation. All other conditions are the same as in Figure 8(a). An error of $\Omega_{err} = (\phi = 10^\circ, \theta = 0^\circ)$ was assumed, i.e. 10° in azimuth. By comparing Figures 9 to Figures 8(a), a clear degradation in ITD and ILD performance for both d-BSM and COM is observed. It can be observed that the d-BSM method is degraded less in its ITD performance compared to COM, and now both methods perform similarly. In addition it can be observed that for both d-BSM and COM methods, the ITD and ILD performance is better than the performance of the BSM method. However, the margin in performance between these two methods and the BSM has been reduced due the assumed DOA error. This can be explained by the robustness of the BSM method that doesn't rely on any DOA estimation. The degradation in performance of the d-BSM and COM can be explained by observing Eq. (10). As this equation represents beamforming, and assuming the look direction is incorrect, the

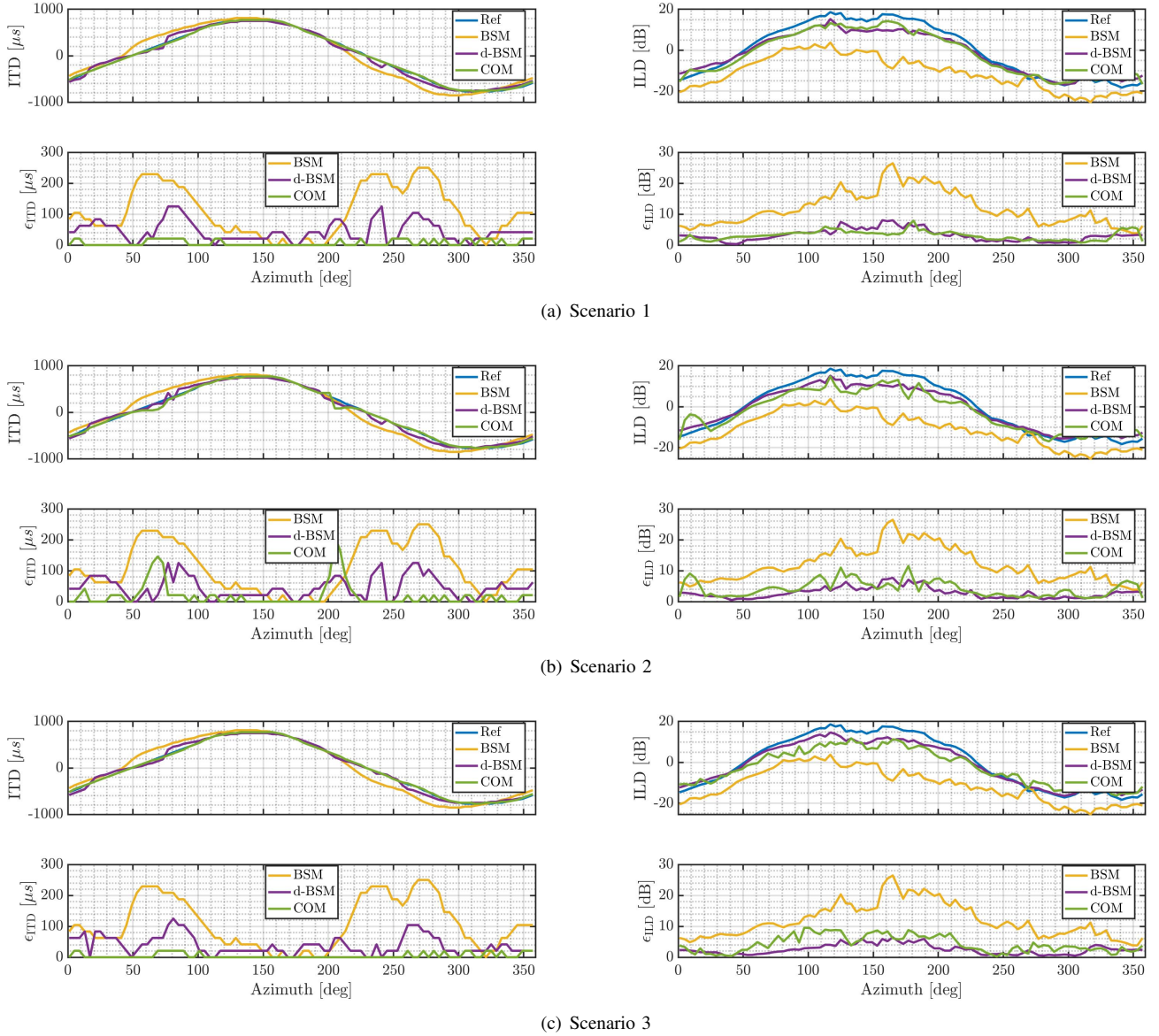


Fig. 8. The ITD on the left and ILD on the right evaluated using the direct sound component of the three different scenarios described in Table I. The orange line represents the BSM method, the purple line corresponds to the d-BSM approach, and the green line depicts the COM approach. ITD and ILD errors are also presented, as defined in Section IV-C. A 50° head rotation was employed.

beamformer will produce a degraded estimation of the source signal.

F. Performance at directions away from source DOA

In this subsection, the ILD and ITD performance of the different methods will be calculated for a specific case. In this case, a single source DOA is used for computing the filters, but analysis is performed in all azimuth directions, i.e. also away from source DOA. This analysis is important since it compares the performance of the different methods in directions other than source DOA, which may also be important, e.g. due to an onset of a source in these directions. The calculation of the ILD and ITD in this chapter can also be divided into two parts. First, a source in a room was simulated generating scenario 1

in Table I. The recorded signals at the array were then used to compute filters for the methods as described in Section V-B. In this case, the source was placed at $\Omega = (40^\circ, 90^\circ)$ relative to the array. Now, using the same filters, binaural signals were computed and ILD and ITD were calculated as defined in Section IV-C, for sound sources in free-field scanning all azimuth directions, and an elevation of 90° .

Figure 10 illustrates the performance of ILD and ITD as detailed above with a 50° rotation of the head. Figure 10 shows that while the methods show similar results, some important observations can be made. It can be seen that while the ILD performance of the three methods is similar in most directions, on the direct source direction, 40° , both d-BSM and COM possess a lower error than the BSM, as expected. Also note

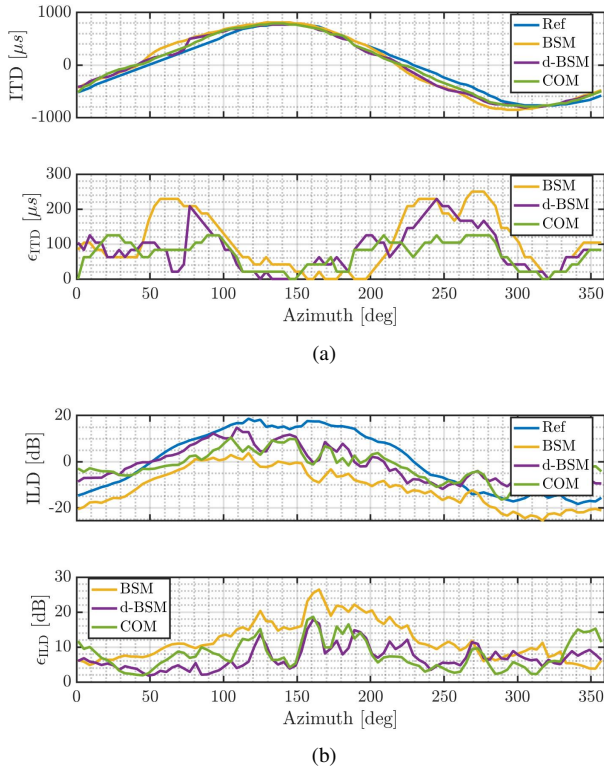


Fig. 9. The ITD (a) and ILD (b) evaluated using the direct sound component of scenario 1 in Table I. The orange line represents the BSM method, the purple line corresponds to the d-BSM approach, and the green line depicts the COM approach. ITD and ILD errors are also presented, as defined in Section IV-C. An error of $\Omega_{err} = (\phi = 10^\circ, \theta = 0^\circ)$ and a 50° head rotation were employed.

that for the COM method, there is a slightly higher error in the directions opposite from the source, e.g. around 220° , while the d-BSM performance remains consistent with the BSM method in those directions. Furthermore, a discernible trade-off can be revealed wherein the enhancement of BSM performance in the DOA of a sound source is counterbalanced by a marginal decrement in performance across other directions. In particular, d-BSM performs better in directions away from the source than COM.

VI. LISTENING EXPERIMENT

The simulation results in the previous section offer valuable insights into the objective performance of the different BSM approaches, but they do not fully capture how these differences are perceived by human listeners. This section describes a listening experiment designed to subjectively compare the quality of the BSM, d-BSM, and COM methods.

A. Setup

The setup in this experiment is based on a simulation of a point source inside a room according to scenario 1 described in Table I. The source is positioned at an angle of $\Omega_d = (40^\circ, 90^\circ)$ around the array, which was also simulated as described in Section V-A, i.e. a semi-circular array with 6 microphones. The room impulse response from the source to

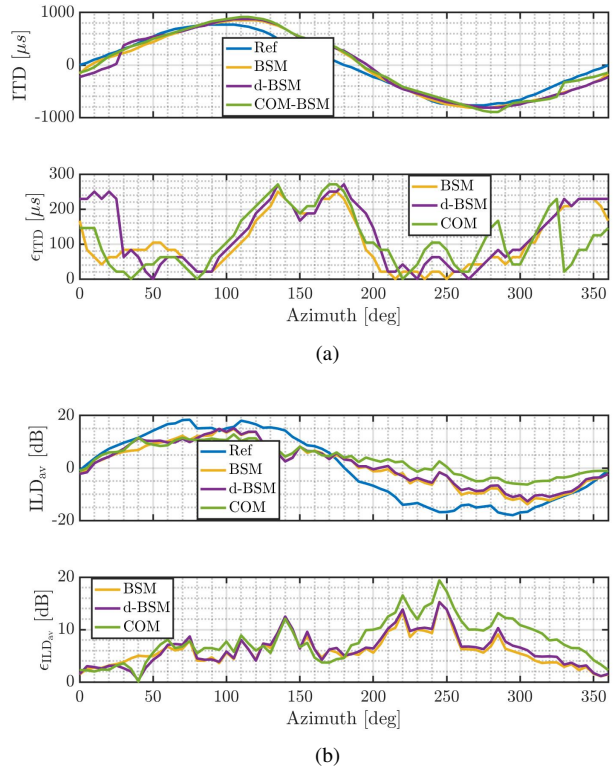


Fig. 10. The ITD (a) and ILD (b) of scenario 1 in Table I, with the direct source positioned at a single direction of 40° . The orange line represents the BSM method, the purple line corresponds to the d-BSM approach, and the green line depicts the COM approach. ITD and ILD errors are also presented, as defined in Section IV-C. 50° head rotation was employed.

the array microphones was simulated using the image method [18] in MATLAB [41]. Microphone signals were generated by convolving the room impulse responses with the speech signal detailed in Table I. HRTF was also used as detailed in Section V-A, including head rotations.

B. Methodology

The binaural signals in this experiment were generated according to Section V-B. The study employed the Multiple Stimuli with Hidden Reference and Anchor (MUSHRA) test [27]. The test featured two MUSHRA screens: both with 50° head rotation, one with an error of 10° in the estimation of speaker direction, as shown in Section V-E and one without. Within each screen, the reference signal was a HOA signal of order $N = 14$, detailed in Section V-B. Each screen included the following four test signals: the hidden reference (HOA), the anchor BSM, d-BSM, and COM, implemented as detailed in Section V-B. Ten subjects, all reported to have normal hearing, participated in the study and were presented with MUSHRA screens and signals in a randomized sequence. They evaluated the similarity of each test signal to the reference signal based on overall quality, encompassing spatial and timbral characteristics. Scores ranged from 0 to 100, with 100 indicating that the test signal was indistinguishable from the reference. In addition, headphone compensation filters cited

in [18] were utilized. Prior to the listening test, participants underwent two training stages: the first familiarized them with the scoring criteria, while the second introduced them to the test signals without requiring scoring. A Repeated Measures ANalysis of VAriance (RM-ANOVA) [42] with two within-subject factors and their interaction was conducted on the scores.

C. Results

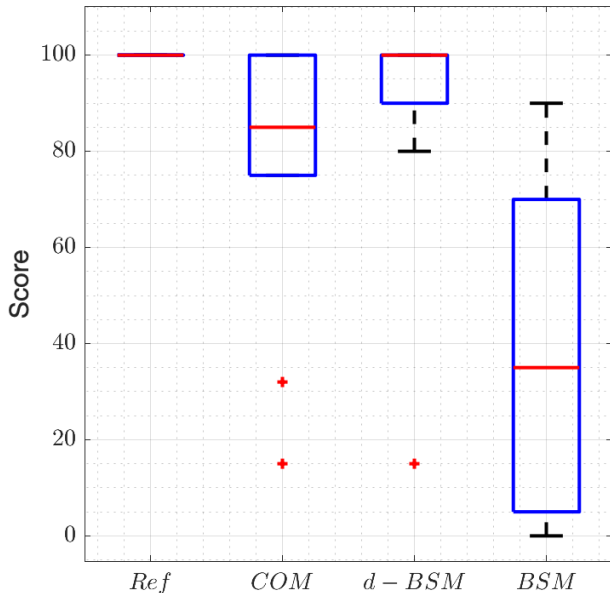


Fig. 11. Similarity to the reference with respect to overall quality, displayed in a box plot, comparing four signals without estimation error: Reference, COM, d-BSM, and BSM, generated as explained in Section VI-A. In the plot, the red line indicates the median, the box edges denote the 25th and 75th percentiles, and the whiskers represent the range of values, excluding outliers.

Figure 11 displays the results of the listening experiment conducted as described above, assuming no estimation error. The reference value consistently received 100 points with no variance, indicating it was identified correctly every time. Both the COM and d-BSM methods received higher scores than the BSM, suggesting an improvement. The RM-ANOVA analysis indicated a significant main effect, with $F(3, 27) = 8.7$, $p < 0.001$, and $\eta_p^2 = 0.4918$. Due to this significant effect, a post-hoc test with Bonferroni correction was performed for further analysis. Pairwise comparisons of the estimated marginal means showed no significant difference between the reference and the COM and d-BSM methods, with a mean difference of 11.5 and 22.8, respectively, and $p > 0.2425$. The most significant difference was between the BSM and the reference, with $p < 0.001$ and a mean difference of 61.7. These results suggest that the adaptive methods improved the BSM performance in this case.

Figure 12 shows the results of the listening experiment conducted as described above, assuming a 10° error in the

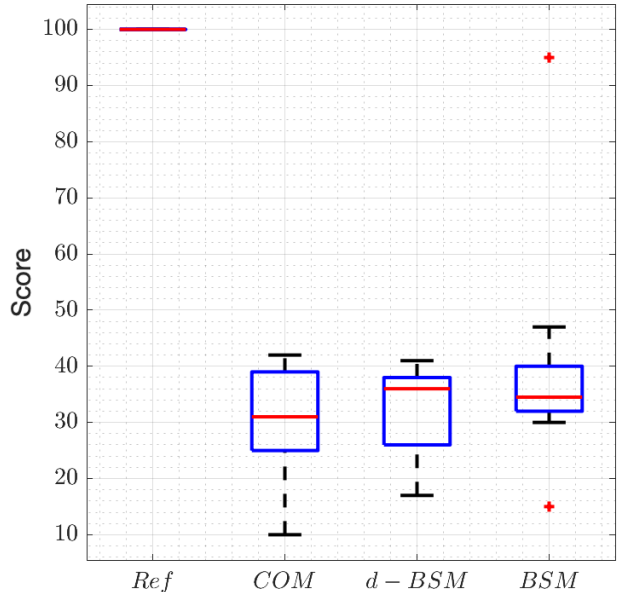


Fig. 12. Similarity to the reference with respect to overall quality, displayed in a box plot, comparing four signals with 10° of error in the estimation of speaker direction: Reference, COM, d-BSM, and BSM, generated as explained in Section VI-A. In the plot, the red line indicates the median, the box edges denote the 25th and 75th percentiles, and the whiskers represent the range of values, excluding outliers.

estimation of speaker direction. Again, the reference value consistently received a score of 100 with no variance, as expected. Both the COM, d-BSM, and BSM methods received similar scores. The RM-ANOVA analysis indicated a significant main effect, with $F(3, 27) = 65.44$, $p < 0.001$, and $\eta_p^2 = 0.88$. Due to this significant effect, a post-hoc test with Bonferroni correction was performed for further analysis. Pairwise comparisons of the estimated marginal means showed no significant difference between the BSM, COM, and d-BSM methods, with a mean difference smaller than 9 and $p = 1$ for all of them. The most significant difference was between the reference and all other methods, with $p < 0.001$ and a mean difference higher than 60. These results suggest that when incorporated with estimation error, both d-BSM and COM converge to the BSM performance.

VII. CONCLUSIONS

This paper offers several significant contributions to the field of binaural signal matching and its application with wearable microphone arrays. First, a new performance metric for BSM, termed the “directional error,” is introduced. This metric quantifies the expected relative error as a function of sound source direction, revealing that BSM errors are highly dependent on the DOA of sound sources, which is closely related to the HRTF magnitude. This behavior was further validated using ITD and ILD analysis. Additionally, the paper presents, analyzes, and compares two approaches that incorporate signal

information into the BSM method, specifically focusing on source DOA. These methods effectively address the limitations imposed by the directional behavior of BSM, demonstrating improved performance across all source directions. This enhanced performance was also confirmed through ITD and ILD analysis. Furthermore, the performance analysis revealed a trade-off where enhancing BSM performance for the DOA of a sound source leads to a slight decrease in performance across other directions. One of the proposed methods showed superior performance in directions away from the source and was found to be more robust to errors in the estimation of DOA. Finally, the paper includes a comprehensive simulation study and a listening experiment that validate the accuracy and quality of the different methods using a wearable microphone array. The results confirm the effectiveness of the proposed approaches and highlight their potential for practical applications. Despite these advances, several limitations remain. The performance of the proposed methods can be significantly affected by errors in DOA estimation, which was evident from the robustness analysis. Additionally, the methods were primarily tested in controlled environments, and their performance in more complex real-world scenarios remains to be fully explored. Future work could focus on improving DOA estimation accuracy to further enhance the robustness of the proposed methods. Additionally, extending the validation of these methods to diverse and dynamic real-world environments would be valuable. Investigating the integration of these methods with other spatial audio processing techniques could also offer new insights and improvements in binaural signal reproduction.

VIII. ACKNOWLEDGMENT

This work was partially supported by Reality Labs Research @ Meta.

REFERENCES

- [1] G. Richard et al., "Audio Signal Processing in the 21st Century: The important outcomes of the past 25 years," *IEEE Signal Processing Magazine*, vol. 40, no. 5, pp. 12–26, July 2023.
- [2] B. Rafaely et al., "Spatial audio signal processing for binaural reproduction of recorded acoustic scenes—review and challenges," *Acta Acustica*, 2022.
- [3] Z. Ben-Hur, F. Brinkmann, J. Sheaffer, S. Weinzierl, and B. Rafaely, "Spectral equalization in binaural signals represented by order-truncated spherical harmonics," *The Journal of the Acoustical Society of America*, vol. 141, no. 6, pp. 4087–4096, 2017.
- [4] M. A. Gerzon, "Ambisonics in multichannel broadcasting and video," *Journal of the Audio Engineering Society*, vol. 33, no. 11, pp. 859–871, 1985.
- [5] A. M. O'Donovan, D. N. Zotkin, and R. Duraiswami, "Spherical microphone array based immersive audio scene rendering," *International Community for Auditory Display*, 2008.
- [6] W. Song, W. Ellermeier, and J. Hald, "Using beam-forming and binaural synthesis for the psychoacoustical evaluation of target sources in noise," *The Journal of the Acoustical Society of America*, vol. 123, no. 2, pp. 910–924, 2008.
- [7] P. Calamia, S. Davis, C. Smalt, and C. Weston, "A conformal, helmet-mounted microphone array for auditory situational awareness and hearing protection," in *2017 IEEE Workshop on Applications of Signal Processing to Audio and Acoustics (WASPAA)*, 2017, pp. 96–100.
- [8] I. Ifergan and B. Rafaely, "On the selection of the number of beamformers in beamforming-based binaural reproduction," *J AUDIO SPEECH MUSIC PROC*, 6, 2022.
- [9] E. Rasumow, M. Blau, M. Hansen, S. Doclo, S. van de Par, D. Puschel, and V. Mellert, "Smoothing head-related transfer functions for a virtual artificial head," in *Acoustics 2012*, 2012.
- [10] C. Schorkhuber, M. Zaunschirm, and R. Holdrich, "Binaural rendering of ambisonic signals via magnitude least squares," in *Proceedings of the DAGA*, vol. 44, 2018, pp. 339–342.
- [11] E. Rasumow, M. Blau, S. Doclo, M. Hansen, D. Puschel, V. Mellert et al., "Perceptual evaluation of individualized binaural reproduction using a virtual artificial head," *Journal of the Audio Engineering Society*, vol. 65, no. 6, pp. 448–459, 2017.
- [12] Z. Ben-Hur, D. L. Alon, R. Mehra and B. Rafaely, "Binaural Reproduction Based on Bilateral Ambisonics and Ear-Aligned HRTFs," *IEEE/ACM Transactions on Audio, Speech, and Language Processing*, vol. 29, pp. 901–913, 2021.
- [13] L. Madmoni, J. Donley, V. Tourbabin, and B. Rafaely, "Beamforming-based binaural reproduction by matching of binaural signals," in *Audio Engineering Society Conference: 2020 AES International Conference on Audio for Virtual and Augmented Reality*. Audio Engineering Society, 2020.
- [14] H. L. Van Trees, *Optimum array processing: Part IV of detection, estimation, and modulation theory*, John Wiley & Sons, 2004.
- [15] E. B. Saff and A. B. J. Kuijlaars, "Distributing many points on a sphere," *The mathematical intelligencer*, vol. 19, no. 1, pp. 5–11, 1997.
- [16] B. Rafaely, *Fundamentals of spherical array processing*, vol. 8, Springer, 2015.
- [17] B. Bernschutz, "A spherical far field HRIR/HRTF compilation of the neumann KU 100," in *Proceedings of the 40th Italian (AIA) annual conference on acoustics and the 39th German annual conference on acoustics (DAGA) conference on acoustics*. AIA/DAGA, 2013, p. 29.
- [18] J. B. Allen and D. A. Berkley, "Image method for efficiently simulating small-room acoustics," *The Journal of the Acoustical Society of America*, vol. 65, no. 4, pp. 943–950, 1979.
- [19] J. S. Garofolo, L. F. Lamel, W. M. Fisher, J. G. Fiscus, D. S. Pallett, N. L. Dahlgren, and V. Zue, "TIMIT acoustic-phonetic continuous speech corpus," *Linguistic Data Consortium*, vol. 10, no. 5, pp. 0, 1993.
- [20] L. Madmoni, J. Donley, V. Tourbabin and B. Rafaely, "Binaural Reproduction From Microphone Array Signals Incorporating Head-Tracking," *2021 Immersive and 3D Audio: from Architecture to Automotive (I3DA)*, 2021, pp. 1-5.
- [21] V. Pulkki, "Directional Audio Coding in Spatial Sound Reproduction and Stereo Upmixing," *Audio Engineering Society Paper 7-1*, 2006.
- [22] L. McCormack, and A. Politis, "SPARTA & COMPASS: Real-Time Implementations of Linear and Parametric Spatial Audio Reproduction and Processing Methods," *journal of the audio engineering society*, Paper 111, 2019.

- [23] V. Pulkki, and M. Karjalainen, "Communication Acoustics: An Introduction to Speech, Audio, and Psychoacoustics," book, 2015.
- [24] L. McCormack, A. Politis, R. Gonzalez, T. Lokki and V. Pulkki, "Parametric Ambisonic Encoding of Arbitrary Microphone Arrays," in *IEEE/ACM Transactions on Audio, Speech, and Language Processing*, vol. 30, pp. 2062-2075, 2022.
- [25] A. Politis, S. Tervo and V. Pulkki, "COMPASS: Coding and Multi-directional Parameterization of Ambisonic Sound Scenes," 2018 IEEE International Conference on Acoustics, Speech and Signal Processing (ICASSP), 2018, pp. 6802-6806
- [26] K. Setsompop, L.L. Wald, V. Alagappan, B.A. Gagoski, E. Adalsteinsson, "Magnitude least squares optimization for parallel radio frequency excitation design demonstrated at 7 Tesla with eight channels." *Magnetic Resonance in Medicine: An Official Journal of the International Society for Magnetic Resonance in Medicine* 59.4, 2007, pp. 908-915.
- [27] ITU-Recommendation, "Method for the subjective assessment of intermediate quality level of coding systems," ITU-R BS, pp. 1534-1, 2003.
- [28] M. Moakher, "A differential geometric approach to the geometric mean of symmetric positive-definite matrices," *SIAM journal on matrix analysis and applications*, 2005, 26.3: 735-747.
- [29] S. Hermon, V. Tourbabin, Z. Ben-Hur, J. Donley, B. Rafaely, "Binaural signal matching with an arbitrary array based on a sound field model". *Audio Engineering Society Conference: AES 2022 International Audio for Virtual and Augmented Reality Conference*. Audio Engineering Society, 2022.
- [30] A. Brughera, L. Dunai, and W. M. Hartmann, "Human interaural time difference thresholds for sine tones: The high-frequency limit," *The Journal of the Acoustical Society of America*, vol. 133, no. 5, pp. 2839-2855, 2013.
- [31] E. A. Macpherson and J. C. Middlebrooks, "Listener weighting of cues for lateral angle: the duplex theory of sound localization revisited," *The Journal of the Acoustical Society of America*, vol. 111, no. 5, pp. 2219-2236, 2002.
- [32] O. L. Frost, "An algorithm for linearly constrained adaptive array processing," *Proc. IEEE*, vol. 60, no. 8, pp. 926-935, Aug. 1972.
- [33] A. Andreopoulou and B. F. Katz, "Identification of perceptually relevant methods of inter-aural time difference estimation," *The Journal of the Acoustical Society of America*, vol. 142, no. 2, pp. 588-598, 2017.
- [34] B. Xie, *Head-related transfer function and virtual auditory display*. J.Ross Publishing, 2013
- [35] M. Slaney, "Auditory toolbox," *Interval Research Corporation, Tech.Rep.*, vol. 10, no. 1998, p. 1194, 1998.
- [36] P. W. Kassakian, Section 5.3.1, "Convex approximation and optimization with applications in magnitude filter design and radiation pattern synthesis," Ph.D. dissertation, University of California, Berkeley Berkeley, CA, 2006.
- [37] D. Menzies and M. Al-Akaidi, "Nearfield binaural synthesis and ambisonics," *The Journal of the Acoustical Society of America*, vol. 121, no. 3, pp. 1559-1563, 2007.
- [38] M. Z. U. Khan, A. N. Malik, F. Zaman, et al., "Robust LCMV Beamformer for Direction of Arrival Mismatch Without Beam Broadening," *Wireless Pers Commun*, vol. 104, pp. 21-36, 2019.
- [39] L. H. Loisel, M. F. Dorman, W. A. Yost, S. J. Cook, and R. H. Gifford, "Using ILD or ITD cues for sound source localization and speech understanding in a complex listening environment by listeners with bilateral and with hearing-preservation cochlear implants," *Journal of Speech, Language, and Hearing Research*, vol. 59, no. 4, pp. 810-818, 2016.
- [40] Klumpp, R. G., and Eady, H. R. "Some measurements of interaural time difference thresholds," *The Journal of the Acoustical Society of America*, vol 28, pp.859-860, 1956.
- [41] MATLAB, version 9.10.0 (R2021a). Natick, Massachusetts: The Math-Works Inc., 2021.
- [42] H. Keselman, J. Algina, and R. K. Kowalchuk, "The analysis of repeated measures designs: a review," *British Journal of Mathematical and Statistical Psychology*, vol. 54, no. 1, pp. 1-20, 2001.
- [43] L. Madmoni, Z. Ben-Hur, J. Donley, V. Tourbabin, B. Rafaely, "Design and Analysis of Binaural Signal Matching with Arbitrary Microphone Arrays." arXiv preprint arXiv:2408.03581, 2024.
- [44] A. Berger, Z. Ben-Hur, J. Donley, V. Tourbabin, B. Rafaely. "Performance Analysis Of Binaural Signal Matching (BSM) in the Time-Frequency Domain". arXiv preprint arXiv:2311.13390, 2023
- [45] L. McCormack, N. Meyer-Kahlen, D. L. Alon, Z. Ben-Hur, S. V. Amengual Garí, and P. Robinson, "Six-degrees-of-freedom binaural reproduction of head-worn microphone array capture," *Journal of the Audio Engineering Society*, vol. 71, no. 10, pp. 638-649, 2023.
- [46] B. Stahl and S. Riedel, "Perceptual comparison of dynamic binaural reproduction methods for sparse head-mounted microphone arrays," *Journal of the Audio Engineering Society*, vol. 72, pp. 442-454, 2024.